Epitaxial $CuInSe_2$ thin films grown by molecular beam epitaxy and migration enhanced epitaxy

K. Abderrafi[1,2,3], R.Ribeiro-Andrade[1,4], N. Nicoara[1,2], M.F. Cerqueira[1,5], M. Gonzalez Debs[1], H. Limborço[1,4], P.M.P. Salomé[1], J.C. Gonzalez[4], F. Briones[2], J.M. Garcia[2], and S. Sadewasser[1]

[1] *International Iberian Nanotechnology Laboratory, Av. Mestre José Veiga s/n, 4715-330 Braga, Portugal*

[2] *Instituto de Microelectrónica de Madrid (CNM-CSIC), Isaac Newton 8, E-28760 Tres Cantos, Madrid, Spain*

[3] *University of Casablanca, Marocco*

[4] *Departamento de Física, Universidade Federal de Minas Gerais, Belo Horizonte, 31270-901, Brasil*

[5] *Centro de Física, Universidade do Minho, Campus de Gualtar, 4710-057 Braga, Portugal*

Email address: Kamal.Abderrafi@inl.int, Sascha.Sadewasser@inl.int

Abstract

While $CuInSe_2$ chalcopyrite materials are mainly used in their polycrystalline form to prepare thin film solar cells, epitaxial layers have been used for the characterization of defects. Typically, epitaxial layers are grown by metal-organic vapor phase epitaxy or molecular beam epitaxy (MBE). Here we present epitaxial layers grown by migration enhanced epitaxy (MEE) and compare the materials quality to MBE grown layers. $CuInSe_2$ layers were grown on GaAs (001) substrates by co-evaporation of Cu, In, and Se using substrate temperatures of 450 ºC, 530 ºC, and 620 ºC. The layers were characterized by high resolution X-ray diffraction (HR-XRD), high-resolution transmission electron microscopy (HRTEM), Raman spectroscopy, and atomic force microscopy (AFM). HR-XRD and HR-TEM show a better crystalline quality of the MEE grown layers, and Raman scattering measurements confirm single phase $CuInSe_2$. AFM shows the previously observed faceting of the (001) surface into {112} facets with trenches formed along the [110] direction. The surface of MEE-grown samples appears smoother compared to MBE-grown samples, a similar trend is observed with increasing growth temperature.

Keywords: A3: Migration enhanced epitaxy; A3: Molecular beam epitaxy; B2:

Semiconducting ternary compounds; A1: Crystal structure; A1: Surface

Structure.

1. Introduction

$CuInSe_2$ (CISe) and $Cu(In,Ga)Se_2$ chalcopyrite semiconductors have been studied intensively during the last decades to push the power conversion efficiency of thin film solar cells closer to the theoretical limit. Reaching 22.6% efficiency [1], they are the most efficient polycrystalline thin-film solar cells available today [2]. The epitaxial growth of CISe on single crystal substrates, including GaAs [3-5], Si [6], Ge [5,7] GaP [8], GaN [9], and ZnSe [10] has been investigated by different groups. Also the improvement of the growth mode with different deposition techniques [11-13] has been investigated to grow epitaxial layers of $CuInSe_2$, in which a lattice–matched substrate results in a reduction of structural defects and roughness in the CISe films.

Usually, for III-V or II-VI compound semiconductors the epitaxial growth occurs in a layer-by-layer manner and the surface of the growing film can be obtained ideally flat if the surface migration rate of the impinging atoms is high and if the thermodynamics parameters, such as surface bond–strengths and substrate temperature, favor abrupt interfaces [14]. In such conditions the growth proceeds by the formation of small monolayer-thick islands and subsequent lateral growth between these islands to complete the monolayer growth. However, this ideal layer-by-layer growth nearly never occurs in the epitaxial growth of I-III-VI_2 compound semiconductors because of the limited surface migration rate of the adatoms and also because the surface stability depends on the film stoichiometry, i.e. the density of Cu vacancies [15]. Typically, the surface of epitaxial layers of CISe, $Cu(In,Ga)Se_2$, or $CuGaSe_2$ grown onto GaAs (001) breaks up into $\{112\}_{tet}$ facets [16]. Such samples show significant surface roughness that can be up to tens of nanometers when conventional molecular beam epitaxy (MBE) or metal organic vapor phase epitaxy (MOVPE) are used [15, 17].

To control the defect formation and the surface flatness for epitaxial III-V and II-VI semiconductors it is preferred to use migration-enhanced epitaxy (MEE) to substitute the conventional MBE growth mode [18]. The MEE growth mode was developed in 1986 by Y. Horikoshi [19] and is illustrated in Fig. 1 in comparison to the conventional MBE growth mode. Migration enhancement is also expected in nucleation-enhanced molecular beam epitaxy (NEMBE), as proposed by Briones et al. [20] during the As_4 suspension periods in III-V growth.

In this growth mode, the deposition produces 2D islands on the growing surface, and this provides several steps and kinks that efficiently absorb metal atoms deposited in the successive cycles. Since the migration distance is quite large in MEE [18], new islands will not be formed unless the growth of the base layer is completed. Thus, the roughness of the MEE grown surface is expected to be on the order of one monolayer.

Despite the advantages of this deposition method and its accuracy, there are only few studies that investigate the growth of epitaxial layers of chalcopyrite thin films using MEE growth [21, 22]. Here, we present epitaxial CISe layers grown by MEE and compare the materials quality to MBE grown layers. $CuInSe_2$ layers were grown on GaAs (001) substrates by co-evaporation of Cu, In, and Se using different substrate temperatures. In contrast to MBE deposition, where all elements are evaporated simultaneously, in MEE deposition cycles of alternating (Cu+In) and (Se) deposition of 2 seconds each are repeated, maintaining all other conditions equal. For comparison, the layers were characterized by high resolution X-ray diffraction (HR-XRD), high-resolution transmission electron microscopy (HRTEM), Raman spectroscopy, and atomic force microscopy (AFM).

2. Experimental

$CuInSe_2$ layers were grown on GaAs (001) substrates in an Omicron EVO-50 MBE equipped with a reflection high-energy electron diffraction (RHEED) using an acceleration voltage of 15 kV, a current of 1.45 mA, and an incident angle of 1.5º for in-situ observation. Selenium (Se) is evaporated using a valved cracker cell (MBE-Komponenten) and Cu and In are evaporated using conventional hot-lip Knudsen cells (MBE-Komponenten) with low evaporation rates.

Prior to the introduction in the growth chamber, GaAs (001) wafer pieces were In-bonded at 160°C to a holder and heated to 250 ºC during 20 min in the load-lock chamber. The background pressure of the growth chamber was 2.0×10^{-10} mbar. Prior to growth, the native oxide on the GaAs wafer was desorbed by annealing the sample at 520 ºC in the presence of In flux [23, 24], this temperature being above the desorption temperature of Ga_2O [25]. This process was in-situ monitored from the evolution of the intensity of the RHEED specular beam I_{oo} in <110>

azimuth. Once the oxide desorption was observed, the temperature was increased by 20 ºC during 5 min to ensure complete oxide desorption (see Fig. 2 (a) and (b)).

$CuInSe_2$ layers were grown on the treated GaAs (001) substrates by evaporation of Cu, In, and Se using substrate temperatures of 450 ºC, 530 ºC, and 620 ºC. For MBE growth, all elements were evaporated simultaneously, while for MEE growth alternating deposition cycles of (Cu+In) and Se for 2 seconds each were performed. Optimized evaporation rates of Cu and In were kept fixed at $\sim 1.4\times10^{13}$ atoms/cm^{-2}s and $\sim 1.9\times10^{13}$ atoms/cm^{-2}s, respectively, during all processes [26]. Se was evaporated from a valved cracker source with the reservoir at 270 ºC and the cracker stage at 900 ºC. The valve was opened to reach a total background pressure of $\sim 3\times10^{-7}$ mbar during the epitaxial growth to avoid any deficiency of Se in the $CuInSe_2$ layer (the total pressure is dominated by the Se partial pressure). The total deposition rate was determined from the final sample thickness to be ~3 nm/min. The growth duration was 813s for all samples grown by the regular MBE process and for 400 cycles for MEE-grown samples. To improve the homogeneity, the substrates were rotated at 10 rpm. After deposition, samples were allowed to cool slowly to 300 ºC in 15-30 min under a 50% reduced Se flux. The slow cooling rate was necessary to avoid delamination or cracking of the film and the Se ambient was necessary to suppress the thermal decomposition of the films.

The film morphology was studied using scanning electron microscopy (FEI® Dual-Beam Helios 450S) and an atomic force microscope (AFM) (Dimension Icon-Bruker) operated in tapping mode using silicon tips. The average compositions of the layers were determined by energy dispersive X-ray spectroscopy (EDS) in the SEM. To evaluate the crystal structure and epitaxial quality of the grown films high-resolution X-ray diffraction (HR-XRD) was used. HR-XRD measurements were performed using Cu $K\alpha^1$ radiation in a Panalytical XPert PRO MRD system using double-axis high resolution optics with the combination of a Ge (220) double crystal and a multilayer X-ray mirror in the incident beam and a parallel-plate collimator with $\delta(\Theta) = 1.6\times10^{-3}$ rad resolution in the diffracted beam. The crystalline phase of the layers was also studied by Raman spectroscopy carried out on an Alpha 300 R confocal Raman microscope (Witec) using a 532 nm Nd-YAG laser for excitation. The laser beam with P = 1 mW was focused on the sample by a 50x lens (Zeiss), and the spectra were collected with 1800 g/mm grating using 10 acquisitions with 2 s acquisition time. A Jeol 2100 LaB6 80-200kV operating at

200 kV was used to acquire high resolution transmission electron microscopy (HR-TEM) images and a FEI ChemiSTEM 80-200kV with probe correction operating at 200 kV was used to perform the energy dispersive spectroscopy (EDS) analysis. The cross-sectional TEM specimens were prepared by focused ion beam (FIB, FEI-Helios 450 S). The FIB milling was performed with accelerating voltage of 30 kV to cut the samples roughly and a subsequent refinement using 2 kV accelerating voltage for final polishing.

3. Results and discussion

In view of the small lattice mismatch of $\Delta a/a \sim 2.3\%$ for the a-axis of $CuInSe_2$, with respect to the lattice constant of GaAs, $a_{GaAs} = 5.6533$ Å (see Fig. 1 (c)), epitaxial growth is achieved by MBE and MEE mode at different growth temperatures. The growth was studied by RHEED, for which the results are shown exemplarily in Fig. 2 for the sample grown by MEE at 530ºC. The RHEED pattern before the growth (Fig. 2 (a) and (b)) shows a streaky pattern, indicating the absence of indium or gallium droplets and reflecting a clean GaAs (001) surface. At the beginning of $CuInSe_2$ growth, the specular intensity drops considerably after deposition of the first layer of metals (Cu+In). The interaction of this metallic layer with incoming selenium atoms increases the specular intensity again. For the [1-10] azimuth a streaky pattern can be observed indicating that the growth is two dimensional. After the deposition of ~1 nm of CISe material, the RHEED images along the [110], [1-10] and [100] azimuths present spotty patterns, suggesting that the growth becomes predominantly three dimensional (Fig. 2 (c) – (e)). The enlarged spots in Fig. 2 (c)-(h) indicate that the thin film is in the form of 3D epitaxial growth. For the thick film (~32 nm), in addition to the main streaks of CISe, other spots appear near the main streaks indicating a superposition of different azimuth crystallites or twins on the {112} planes [8] (Fig. 2 (f)-(h)).

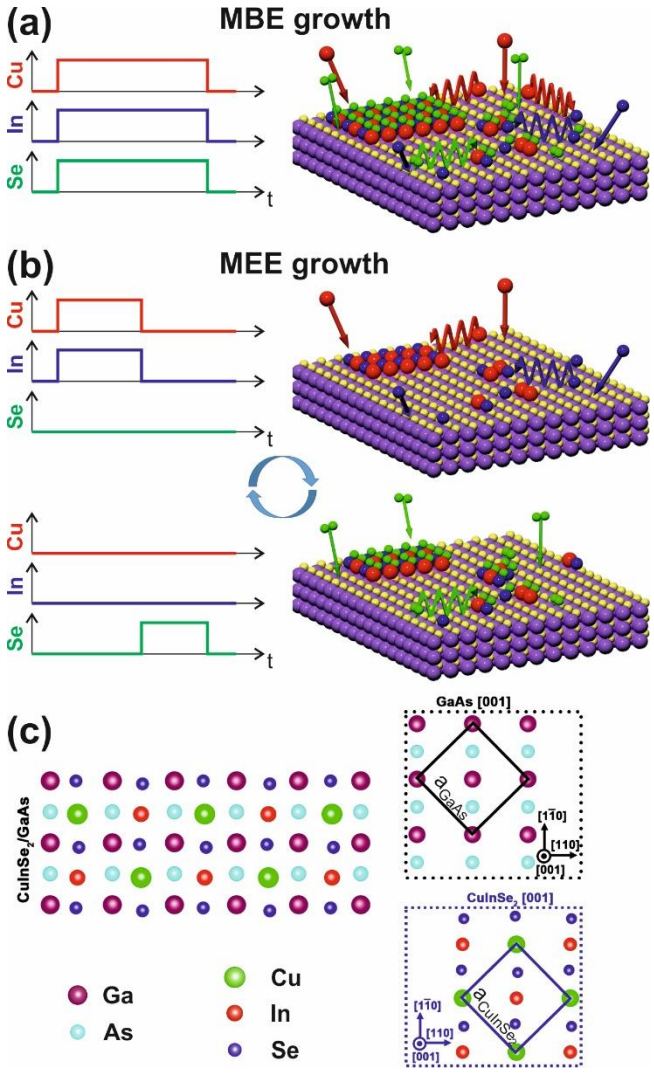

Figure 1: Schematic illustration of the (a) MBE and (b) MEE growth modes. (a) In MBE growth mode all atomic species impinge simultaneously onto the surface, while in (b) MEE mode the metal cations and Se anions impinge separately in a cycled process, thereby increasing significantly the migration length on the surface resulting in an improved layer growth. (c) Illustration of the structure of GaAs and $CuInSe_2$ in the (001) growth plane and the lattice mismatch between the GaAs (001) substrate and the $CuInSe_2$ thin film.

The AFM study performed on the MBE and MEE samples reveal that all samples show a corrugated surface structure forming a periodically faceted surface with trenches along the [110] direction of the GaAs (001) substrate (Fig. 3). A similar surface topography is typically observed in epitaxial thin films and is characteristic of $\{001\}_{tet}$ surfaces of $CuInSe_2$ [15, 28]. Comparing the surface structure of samples prepared at different temperatures using MBE and MEE growth

modes it becomes clear that the dimensions of the periodic structures change with increasing growth temperature.

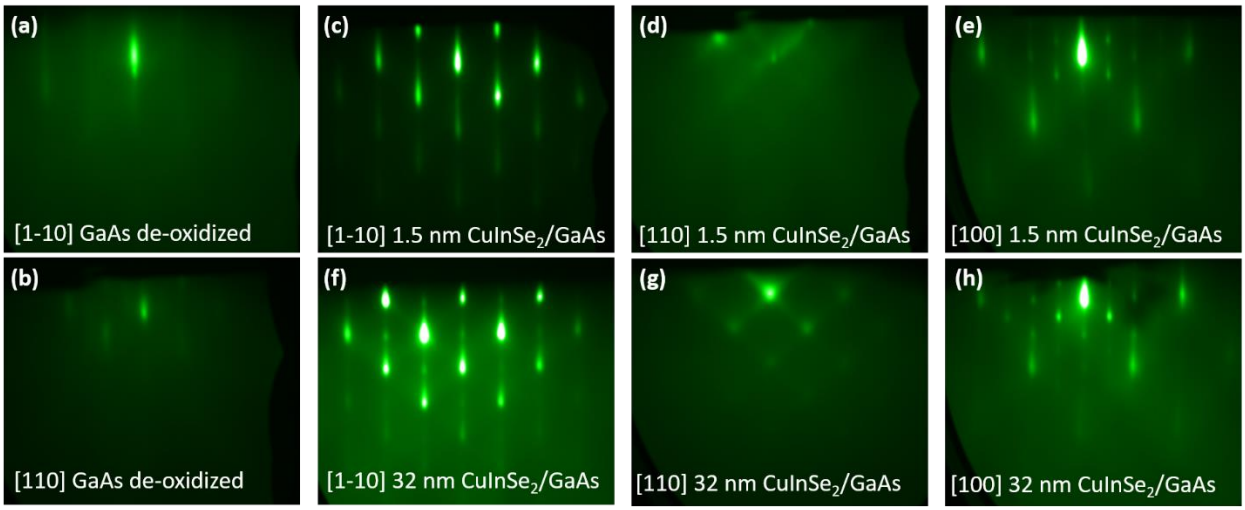

Figure 2: In situ RHEED images of the GaAs (001) surface after oxide removal by depositing In at T_s = 530 °C for (a) the [1-10] and (b) the [110] azimuths. RHEED images after the deposition of ~1.5 nm (18 deposition cycles of (Cu+In) and Se) by MEE at 530 ºC for (c) [1-10], (d) [110], and (e) [100] azimuths with respect to the GaAs substrate. (f) through (h) show RHEED images along the same azimuths for the completed growth of ~32 nm thickness.

For samples grown at high temperature (620 ºC) the topography characteristics of samples deposited by MBE and MEE modes are similar. Both samples show a corrugated surface with the presence of small dispersed droplets, possibly indicating the formation of a trace amount of Cu_{2-x}-Se as an impurity phase (as confirmed by Raman, see below) [29, 30]. The sample grown by classical MBE mode presents a higher density (~10^9 cm^{-2}) of these droplets, in comparison with the MEE sample that shows a lower density by one order of magnitude. Roof-like structures oriented along the [110] direction are observed, several hundreds of nm long, with homogenous width on the order of 10-20 nm. These surface deformations are typically associated with elastic strain relaxation and have been reported previously for other compressively strained heteroepitaxial systems [29]. The formation of this anisotropic structure on the surface of epitaxial CISe thin films is due to surface faceting into long low-energy Se-terminated {112}B facets with short metal-terminated {112}A facets at their ends [28]. The reason is that the surface energy of the {112} surface (Se or metal terminated), $\gamma(112)$, is lower than that of the {001} surface, $\gamma(001)$, in the Cu-poor regime [15, 28]. The size and dimensions of these structures depend on the Cu/In ratio [15].

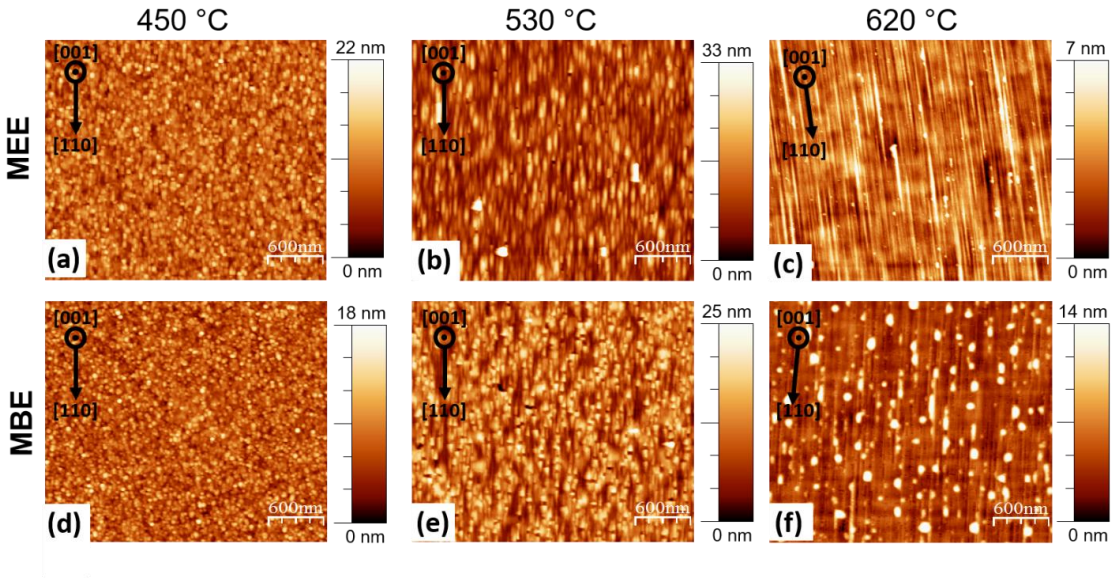

Figure 3: Surface morphology of the $CuInSe_2$ films measured by AFM. (a)-(c) CISe films grown by MEE and (d)-(f) by MBE at (a) and (d) 450 ºC, (b) and (e) 530 ºC and (c) and (f) 620 ºC substrate temperature. All images are 3x3 μm^2.

For samples grown at 530 ºC this corrugated surface structure is maintained, but the size of the periodic structures changes. The roof-like structures become shorter (on the order of 100 - 200 nm) and extend in width and height. These changes are more pronounced in the samples grown by MBE. The MBE samples are characterized by the presence of a high density (3×10^9 cm^{-2}) of rectangular pit-type defects, which have their long axis perpendicular to the [110] direction. The formation of these pit defects is possibly associated with the presence of holes on the GaAs substrate after desorption of the native oxide. For III-N materials, pit-type defects have been found to originate from dislocations at the interface between substrate and film [30, 31]. However, pit-type defects on CISe and $CuIn_3Se_5$ epitaxial films form spontaneously and their geometry is controlled by the relation of the surface energies of the {112}A and {112}B facets [28]. For samples grown by MEE at 530 ºC the pit-type defects are less pronounced (density ~ 3×10^8 cm^{-2}), which can be explained by one of the principal advantages of MEE: when only the cations (Cu+In) are supplied, they have sufficient time to find the preferable nucleation sites, directly suppressing the defect formation and resulting in a well-ordered and smooth surface layer.

At low temperature (450 ºC) the MBE and MEE samples show surfaces with short corrugated structure. The structures are only a few tens of nm long, along the (110) direction of the film. The small size and high density of these structures leads to a higher surface roughness. These smaller structures are a result of the lower surface mobility of the impinging atoms at the lower growth temperature, as has been shown previously [15, 16]. At this temperature, no significant difference between the MBE and MEE samples is observed.

Summarizing, the AFM analysis shows the formation of a corrugated surface structure in form of a periodically faceted surface with trenches along the [110] direction of the GaAs (001) substrate. The reduction of this faceting into {112} surfaces at higher growth temperatures is in agreement with a reduced incorporation of indium and indicates a higher re-evaporation of In at the higher growth temperatures. A lower density of pit-type defects is achieved by the MEE growth mode.

Raman scattering has proven to be a suitable technique for the detection of composition and the presence of secondary phases [32]. To obtain further structural information about the epitaxial $CuInSe_2$ thin films we used Raman spectroscopy. Fig. 4 shows the Raman spectra of the samples grown by MEE and MBE at different substrate temperature, showing that all samples exhibit the chalcopyrite ($CuInSe_2$) structure [33]. At least six peaks are observed in each spectrum, where the most intense line at 175 cm^{-1} is assigned to the A_1 mode of $CuInSe_2$, which results from the motion of Se atoms with the Cu and In atoms remaining at rest [34]. The weaker peaks at 160 cm^{-1} (B1), 215 cm^{-1} (B_2), and 235 cm^{-1} (E_1) are in agreement with the lattice modes of chalcopyrite $CuInSe_2$. The two remaining peaks are related to the GaAs (001) substrate, corresponding to the transverse-optical (TO) mode at 268 cm^{-1} and the longitudinal-optical (LO) mode at 291cm^{-1}. The Raman spectra do not show any sizable signal at 183 cm^{-1} (corresponding to the lattice mode of CuAu-$CuInSe_2$) or at 150 cm^{-1} (corresponding to the vibrational mode of a Cu-poor ordered vacancy compound), confirming a high crystalline quality of the grown films. Only for the CISe thin films grown by MEE and MBE at the lowest temperature of 450 ºC very weak signals of the CuAu-$CuInSe_2$ and OVC are seen in the Raman spectra. Thus, Raman spectroscopy confirms that all samples exhibit the chalcopyrite $CuInSe_2$ structure. The lower peak position and full width at half maximum (FWHM) of the A_1 mode for samples grown by MEE in comparison with MBE samples indicate that the MEE growth method allows for a better crystalline quality of the samples.

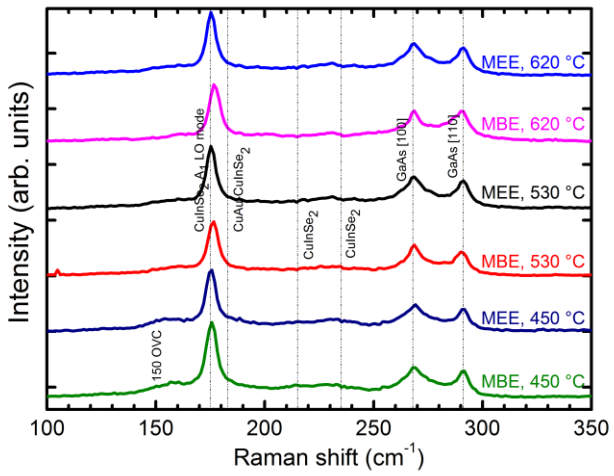

Figure 4: Raman spectra of $CuInSe_2$ thin films grown by MBE and MEE on GaAs (001) substrates at 450 ºC, 530 ºC, and 620 ºC.

Further structural analysis was performed by HR-XRD. Fig. 5 shows the 2Θ/ω scans around the $CuInSe_2$ (008) reflection for the MEE and MBE thin films grown at 450 ºC, 530 ºC, and 630 ºC; the GaAs (004) and $CuInSe_2$ (008) peaks are observed. The thickness of the films is 32 ± 2 nm (as determined from cross sectional TEM imaging). While for MEE-grown samples the HR-XRD spectra indicate that complete relaxation has occurred, the peak position of the $CuInSe_2$ (008) peak in the MBE-grown samples indicates that the layer is not fully relaxed. The latter is in agreement with observations that the critical thickness for relaxation of epitaxial layers is larger than 40 nm [27]. This study indicates that relaxation of the CISe layer grown by MEE occurs at a thickness lower than the relaxation in MBE-grown CISe layers.

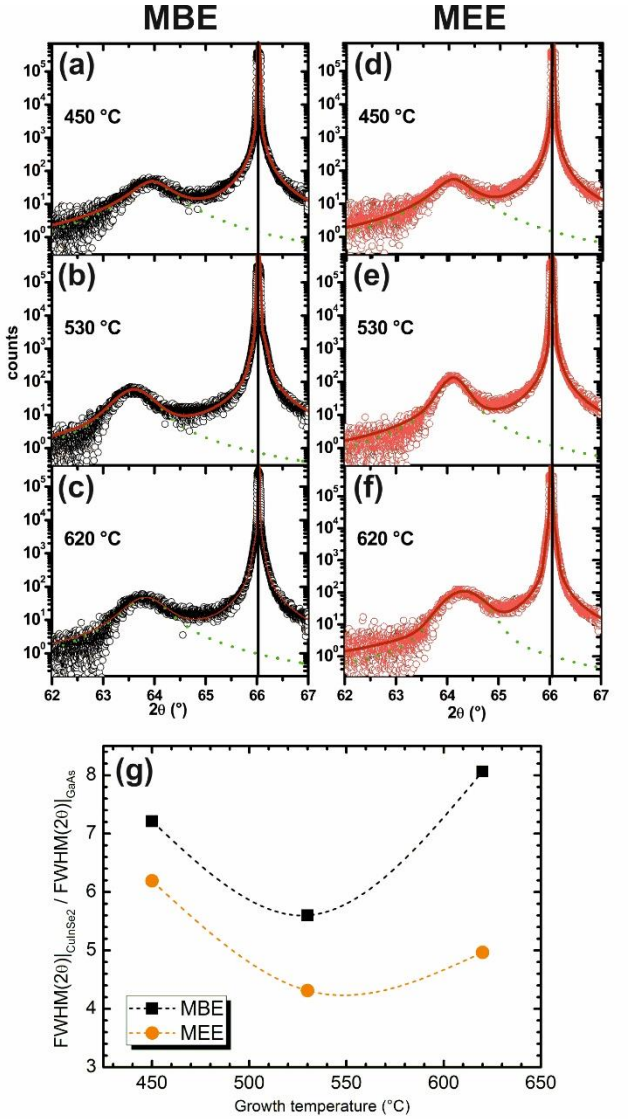

Figure 5: 2Θ/ω scans of $CuInSe_2$ thin films grown on GaAs (001) substrates at (a, d) 450 ºC, (b, e) 530 ºC, and (c, f) 620 ºC by MBE (a, b, c) and MEE (d, e, f). (g) Variation of the ratio (FWHM ($CuInSe_2$ (008))/(FWHM GaAs (004)) as a function of growth substrate temperature.

The calculated misfit ranges from 2.3% to 3.1% depending on the growth temperature. A shift of the HR-XRD peaks to larger Bragg angles for films grown by MEE growth mode is observed, independent of the growth temperature. Thus the MEE samples show a smaller lattice strain and a high crystalline and interfacial quality in comparison to those grown by MBE mode. This lattice strain between the GaAs substrate and $CuInSe_2$ epitaxial layers might play a role in the formation of the corrugated surface observed in the AFM images. Similar phenomena have been

observed in epitaxial films of SiGe grown on GaAs (001) substrates [35], in which the formation of the corrugated surface was also obtained and explained by the elastic relaxation of the interfacial misfit by diffusion of the larger atoms to areas of lower strain [36].

A measure of the crystalline quality of the CISe films grown by MBE and MEE can be determined from the FWHM of the peaks of the rocking curve. The samples grown by MEE mode show consistently smaller FWHM values (Fig. 5). The large FWHM of the $CuInSe_2$ (008) peaks of the MBE samples reflects the presence of a high density of dislocations, a mosaicity, or a curvature in the sample. This result clearly indicates that the best temperature to grow $CuInSe_2$ / GaAs interfaces with a reduced number of dislocations and other defects is around 530 ºC and the use of MEE growth mode is beneficial for this material system.

To further investigate the crystalline quality of the layers we performed HR-TEM measurements. Since the XRD study revealed the best sample quality for a growth temperature of 530 ºC, HR-TEM was performed on the MBE and MEE samples grown at this temperature. Fig. 6 shows cross-sectional images of $CuInSe_2$/GaAs (001) grown by MEE and MBE modes along the [110] zone axis. Both samples clearly show a crystalline transition from the substrate to the CISe layer, confirming epitaxial growth, and the absence of any amorphous layer forming at the interface, in spite of the lattice mismatch between the grown layer and the substrate. However, in both samples misfit dislocations are observed at the interface along the zone axis [110]. Additionally, twin defects are observed at angles of 70.5º and aligned in the directions [1,-1,1] and [-1,1,1]. While in the MBE grown sample these twin defects are concentrated at the interface, with a small portion extending through the CISe film thickness, for the MEE grown sample the density of these defects is low at the interface but most of them extend throughout the CISe film thickness. The interplanar distances of CISe (-1,1,2), (1,-1,2), and (0,0,4) were obtained from power spectra (not shown) generated from four areas in the thin film. The interplanar distances and standard deviation are (0.337±0.001) nm, (0.333±0.004) nm, and (0.295±0.001) nm, respectively, for the MBE sample, and (0.338±0.003) nm, (0.335±0.003) nm, and (0.297±0.001) nm for the MEE sample. These values are in agreement with the tetragonal structure of $CuInSe_2$ [37]. The EDS analysis confirms the chemical composition of $CuInSe_2$ for both samples. From the EDS profiles (Fig. 6 (c) and (f)) a transition region of ~4 nm width can be identified. Finally, for both samples we observe a bright contrast in the HAADF images at the interface between substrate and layer.

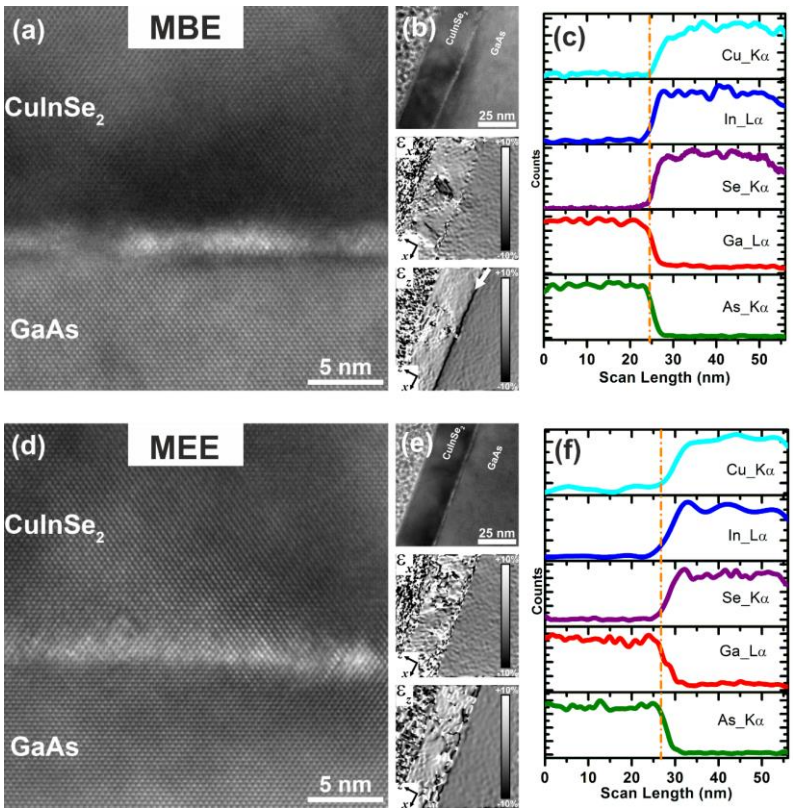

Figure 6: Cross sectional HR-TEM images of $CuInSe_2$/GaAs(001) grown at 530 ºC by (a) MBE and (d) MEE modes. (b, e) The strain in x and z-direction is extracted from a geometrical phase analysis. The composition across the interface, as measured by EDS, is shown for the (c) MBE and (f) MEE sample.

To further investigate the interface, we performed a geometrical phase analysis (GPA) of the images (Fig. 6 (b) and (e)) to produce quantitative measures of strain in the CISe films [38-42]. Briefly, the GPA method consists of filtering the image at a Bragg spot of the Power Spectrum of a TEM lattice image. Then the reference lattice ($[2\pi\vec{g}\cdot\vec{r}]$ term) is subtracted by re-centering the filtered Power Spectrum image around $\vec{g}$ and the phase image is obtained from the imaginary term of the complex image calculated from the inverse Fourier transform. The main limitation of the GPA technique is related to the delocalization effects caused by the defocus, thickness, and (mainly) by the spherical aberration of the objective lens. The analysis was carried out using the STEM CELL package [43] and measuring the local displacement with respect to a reference region (GaAs). In order to characterize the local lattice deformation, the $\vec{g}_1 = [004]_{CIS}//[002]_{GaAs}$ and $\vec{g}_2 = [\bar{1}12]_{CIS}//[\bar{1}10]_{GaAs}$ were selected. Maps of in-plane strain fields ($\varepsilon_x = \left(d_{GaAs}^{[\bar{2}20]} - d_{CIS}^{[\bar{2}20]}\right)/d_{GaAs}^{[\bar{2}20]}$ and $\varepsilon_z = \left(d_{GaAs}^{[002]} - d_{CIS}^{[004]}\right)/d_{GaAs}^{[002]}$) were derived by analyzing the

derivative of the displacement obtained from two phase images ($\vec{g}_1$ and $\vec{g}_2$). The strain maps reveal inhomogeneities in the strain along the CISe films. Abrupt changes in the strain images result from phase unwrapping in the GPA process due to the thickness of the specimen [44] or point to the presence of misfit or twin defects [45, 46]. Nevertheless, large areas in the depicted regions exhibit homogeneous strain values. The strain in the substrate is virtually zero (the +0.01% average *x*-directed strain in the GaAs substrate is statistically indistinguishable from +0.015% average *z*-directed strain in the GaAs in both samples). The strain in the CISe layer is approximately +1% along the *x*-direction and +2.34% along the *z*-direction relative to the GaAs for the MBE sample. In addition, a highly strained layer can be seen with -5.22% strain in average while the ε_z strain map shows approximately +0.37% in average. For the MEE sample the CISe layer shows +1.62% average *x*-directed strain and +2.1% *z*-directed strain with very low strain values for the interface layer with +0.1% *x*-directed and -0.48% *z*-directed. The ε_x and ε_z strain values for the CISe film relative to the substrate do not differ significantly in the two samples, i.e., there is no significant difference of the interplanar spacing between the two thin films. However, the interface layer in the MBE sample contains a biaxial tensile or compressive strain of the interplanar spacing parallel to the GaAs surface, leading to a large number of defects that allows to relax the CISe on the top. This interface layer thickness - called the critical thickness [47, 48] - measures ~3.8 nm in average for the MBE sample and ~1.6 nm for the MEE sample. The biaxial strain is quite low for the MEE sample, possibly due to the reduced thickness or low density of defects of the interface layer which leads also to a low density of defects in the thin film in agreement with the XRD results.

4. Conclusion

Single-phase $CuInSe_2$ epitaxial films were successfully grown on GaAs (001) substrates at different growth temperatures and using two different growth modes, MBE and MEE. The typically observed faceting of the (001) surface into {112} facets with trenches formed along the [110] direction was observed. Samples grown at higher growth temperature exhibit lower roughness. Moreover, the surface appears always smoother for samples grown by MEE mode. Independent of the growth mode, at high growth temperatures the incorporation of indium to form $CuInSe_2$ is limited, leading to an increase of the Cu/In ratio and a decrease in the faceting

of the surface into {112} facets. Additionally, MEE growth results in the reduction of pit-type defects and a better crystalline quality.

Acknowledgements

The authors would like to acknowledge the CAPES (CAPES-INL 04/14), CNPq, and FAPEMIG funding agencies for financial support. We acknowledge the collaboration project with IMM-CSIC (AIC-B-2011-0806). P.M.P.S. acknowledges financial support from EU through the FP7 Marie Curie IEF 2012 Action No. 327367.

References

[1] P. Jackson, R. Wuerz, D. Hariskos, E. Lotter, W. Witte and M. Powalla, Effects of heavy alkali elements in Cu(In,Ga)Se_2 solar cells with efficiencies up to 22.6%, Phys. Status Solidi RRL 10 (2016) 583–586.

[2] M.A. Green, K. Emery, Y. Hishikawa. W. Warta, E.D. Dunlop, D.H. Levi, A.W.Y. Ho-Baillie, Solar cell efficiency tables (version 49), Prog. Photovolt. Res. Appl. 25(2017) 3-13.

[3] B.-H. Tseng, S.-B. Lin, G.-L. Gu, and W. Chen, Elimination of orientation domains and antiphase domains in the epitaxial films with chalcopyrite structure, J. Appl. Phys. 79 (1996) 1391; doi: 10.1063/1.361038.

[4] L.C. Yang, L.J. Chou, A. Agarwal, A. Rockett, Single crystal and polycrystalline $CuInSe_2$ by the hybrid sputtering and evaporation method, Conference Record 22nd IEEE Photovoltaic Specialists Conference - 1991 (Cat. No.91CH2953-8), p 1185-9 vol.2, (1991).

[5] G. Kuhn, B. Schumann, $CuInSe_2$ epitaxial layers with sphalerite structure, Crystal Research and Technology 23 (1988) K40-42.

[6] A.N. Tiwari, S. Blunier, K. Kessler, V. Zelezny and H. Zogg, Direct growth of heteroepitaxial $CuInSe_2$ layers on Si substrates, Appl. Phys. Lett. 65 (1994) 2299. doi: 10.1063/1.112723

[7] B. Schumann, A. Tempel, C. Georgi, G. Kuhn, Heteroepitaxy of $CuInSe_2$ on {111}-oriented germanium, Thin Solid Films 70 (1980) 319-324.

[8] O. Igarashi, Epitaxial growth of $CuInSe_2$ single crystal by halogen transport method, J. Cryst. Growth 130 (1993) 343-356.

[9] C.-H. Shih, I. Lo, S.-T. You, C.-D. Tsai, B.-H. Tseng, Y.-F. Chen, C.-H. Chen, G.Z.L. Hsu, Direct growth of heteroepitaxial $CuInSe_2$ on GaN (0001) by molecular beam epitaxy, Thin Solid Films 574 (2015) 132–135.

[10] A. Hofmann, Ch. Pettenkofer, Surface orientation dependent band alignment for $CuInSe_2$–ZnSe–ZnO, Appl. Phys. Lett. 98 (2011) 113503.

[11] S. Niki, P.J. Fons, A. Yamada, T. Kurafuji, S. Chichibu, H. Nakanishi, W.G. Bi, and C.W. Tu, High quality $CuInSe_2$ films grown on pseudo-lattice-matched substrates by molecular beam epitaxy, Appl. Phys. Lett. 69 (1996) 647; doi: 10.1063/1.117793.
[12] B. Sagnes, A. Salesse, M.C. Artaud, S. Duchemin, J. Bougnot, G. Bougnot, MOCVD growth of $CuInSe_2$: first results, J. Cryst. Growth 124 (1992) 620-627.
[13] T. Walter, H.-W. Schock, Crystal growth and diffusion in $Cu(In,Ga)Se_2$ chalcopyrite thin films, Thin Solid Films 224 (1993) 74-81.
[14] Y.C. Chen, P.K. Bhattacharya and J. Singh, Strained layer epitaxy of InGaAs by MBE and migration enhanced epitaxy — comparison of growth modes and surface quality, J. Cryst. Growth 111 (1991) 228-232.
[15] S. Siebentritt, N. Papathanasiou, J. Albert, and M.Ch. Lux-Steiner, Stability of surfaces in the chalcopyrite system, Appl. Phys. Lett. 88 (2006) 151919. doi: 10.1063/1.2192638.
[16] D. Liao and A. Rockett, Epitaxial growth of $Cu(In,Ga)Se_2$ on GaAs(110), J. Appl. Phys. 91 (2002) 1978. doi: 10.1063/1.1434549.
[17] S. Niki, I. Kim, P.J. Fons, H. Shibata, A. Yamada, H. Oyanagi, T. Kurafuji, S. Chichibu, H. Nakanishi, Effects of annealing on $CuInSe_2$ films grown by molecular beam epitaxy, Sol. En. Mat. Sol. Cells 49 (1997) 319-326.
[18] Y. Horikoshi, M. Kawashima, and H. Yamaguchi, Migration-Enhanced Epitaxy of GaAs and AlGaAs, Jpn. J. Appl. Phys. 27 (1988) 169.
[19] Y. Horikoshi, M. Kawashima, and H. Yamaguchi, Low-Temperature Growth of GaAs and AlAs-GaAs Quantum-Well Layers by Modified Molecular Beam Epitaxy, Jpn. J. Appl. Phys. 25 (1986) L868.
[20] F. Briones, L. Gonzalez, A. Ruiz, Atomic layer molecular beam epitaxy (Almbe) of III–V compounds: Growth modes and applications, Appl. Phys. A 49 (1989) 729. doi:10.1007/BF00617001
[21] B. J. Stanbery, S. Kincal, S. Kim, C. H. Chang, S. P. Ahrenkiel, G. Lippold, H. Neumann, T. J. Anderson and O. D. Crisalle, Epitaxial growth and characterization of $CuInSe_2$ crystallographic polytypes, J. Appl. Phys. 91 (2002) 3598. doi: 10.1063/1.1446234.
[22] S. Thiru, M. Asakawa, K. Honda, A. Kawaharazuk, A. Tackeuchi, T. Makimoto, and Y. Horikoshi, Investigation of $CuGaSe_2$/$CuInSe_2$ double heterojunction interfaces grown by molecular beam epitaxy, AIP Adv. 5 (2015) 027120. doi: 10.1063/1.4908229
[23] L.H. Li, E.H. Linfield, R. Sharma, and A.G. Davies, In-assisted desorption of native GaAs surface oxides, Appl. Phys. Lett. 99 (2011) 061910. doi: 10.1063/1.3623424
[24] D. Fuster, L. Ginés, Y. González, J. Herranz, L. González, Low temperature oxide desorption in GaAs (111)A substrates, Thin Solid Films 537 (2013) 70-75.
[25] Z.R. Wasilewski, J.-M. Baribeau, M. Beaulieu, X. Wu, and G.I. Sproule, J. Vac. Sci. Technol. B 22 (2004) 1534. doi: 10.1016/j.tsf.2013.04.044
[26] The evaporation rates where determined using a water-cooled quartz crystal balance in the position of the substrate.
[27] P. Fons, S. Niki, A. Yamada, M.Uchino, and H. Oyanagi, JCPDS-International Centre for Diffraction Data, Advances in X-ray Analysis, Vol. 43 (2000) 201.

[28] L.-C. Yang, G.S. Chen and A. Rockett, Surface polarities of sputtered epitaxial $CuInSe_2$ and $Cu_1In_3Se_5$ thin films grown on GaAs (001) substrates, Appl. Phys. Lett. 86 (2005) 201907. doi: 10.1063/1.1929071
[29] L Persichetti, A Sgarlata, M Fanfoni and A Balzarotti, Heteroepitaxy of Ge on singular and vicinal Si surfaces: elastic field symmetry and nanostructure growth, J. Phys.: Condens. Matter 27 (2015) 253001.
[30] X.H. Wu, C.R. Elsass, A. Abare, M. Mack, S. Keller, P.M. Petroff, S.P. DebBaars, J.S. Speck, Structural origin of V-defects and correlation with localized excitonic centers in InGaN/GaN multiple quantum wells, Appl. Phys. Lett. 72 (1998) 692. doi: 10.1063/1.120844
[31] K.S. Son, D.G. Kim, H.K. Cho, K.H. Lee, S.W. Kim, K.S. Park, Formation of V-shaped pits in GaN thin films grown on high temperature GaN, J. Cryst. Growth 261 (2004) 50-54. doi: 10.1016/j.jcrysgro.2003.08.075
[32] J.N. Gan, J. Tauc, V.G. Larnbrecht, Jr., and M. Robbins, Raman and infrared spectra of the $(CuInSe_2)_{1-x}$–$(2ZnSe)_x$ system, Phys. Rev. B 13 (1976) 3610. doi: 10.1103/PhysRevB.13.3610
[33] H. Tanino, T. Maeda, H. Fujikake, H. Nakanishi, S. Endo and T. Irie, Raman spectra of $CuInSe_2$, Phys. Rev. B 45 (1992) 13323. doi: 10.1103/PhysRevB.45.13323
[34] H. Neumann, Lattice vibrations in $A^IB^{III}C^{VI}_2$ chalcopyrite compounds, Helvetica Physica Acta 58 (1985) 337-346.
[35] V.I. Vdovin, M. Mühlberger, M.M. Rzaev, F. Schäffler, and T.G. Yugova, Dislocation structure formation in SiGe/Si(001) heterostructures with low-temperature buffer layers, J. Phys.: Condens. Matter 14 (2002) 13313-13318.
[36] J. Tersoff and F.K. Leogues, Competing relaxation mechanisms in strained layers, Phys. Rev. Lett. 72 (1994) 3570. doi: 10.1103/PhysRevLett.72.3570
[37] International Centre for Diffraction Data, datasheet 04-007-4441.
[38] M.J. Hÿtch, E. Snoeck, R. Kilaas, Quantitative measurement of displacement and strain fields from HREM micrographs, Ultramicroscopy 74 (1998) 131-146.
[39] M.J. Hÿtch, J.L. Putaux, J.M. Pénisson, Measurement of the displacement field of dislocations to 0.03 Å by electron microscopy, Nature 423 (2003) 270-273.
[40] M. J. Hÿtch, Analysis of Variations in Structure from High Resolution Electron Microscope Images by Combining Real Space and Fourier Space Information, Microsc. Microanal. Microstruct. 8 (1997) 41-57.
[41] M.J. Hÿtch, L. Potez, Geometric phase analysis of high-resolution electron microscopy images of antiphase domains: Example Cu_3Au, Philos. Mag. A 76 (1997) 1119-1138.
[42] M. J. Hÿtch, M. Gandais, Quantitative criteria for the detection and characterization of nanocrystals from high-resolution electron microscopy images, Philos. Mag. A 72 (1995) 619-634.
[43] V.Grillo, Stemcell Software, http://tem-s3.nano.cnr.it/stemcell.htm
[44] D. Diercks, G. Liang, J. Chung, M. Kaufman, Comparison of convergent beam electron diffraction and geometric phase analysis for strain measurement in a strained silicon device, J. Microscopy 241 (2011) 195-199.

[45] Y. H. Kim, H. J. Park, K. Kim, C. S. Kim, W. S. Yun, J. W. Lee, and M. D. Kim, Strain distribution and interface modulation of highly lattice-mismatched InN/GaN heterostructure nanowires, Appl. Phys. Lett. 95 (2009) 033112.
[46] M. Sennour, S. Lartigue-Korinek, Y. Champion, M. J. Hÿtch, HRTEM study of defects in twin boundaries of ultra-fine grained copper, Philos. Mag. 87 (2007) 1465-1486.
[47] J.W.Matthews and A.E. Blakeslee, Defects in epitaxial multilayers: I. Misfit dislocations, J. Cryst. Growth 27 (1974) 118-125.
[48] R. People and J. C. Bean, Calculation of critical layer thickness versus lattice mismatch for GexSi1−x/Si strained-layer heterostructures, Appl. Phys. Lett. 47 (1985) 322-324.